

Direct conversion of glyceride-based oil into renewable jet fuels

Cheng-Han Lin, Wei-Cheng Wang *

Department of Aeronautics and Astronautics, National Cheng Kung University, Tainan, 70101, Taiwan



ARTICLE INFO

Keywords:

Renewable jet fuel
Hydro-conversion
Ni-based catalyst
SAPO-11 zeolite
Citric acid
Phosphotungstic acid hydrate

ABSTRACT

Hydro-conversion of triglyceride to renewable jet fuel (HRJ) plays an important role in drop-in aviation fuels and has drawn the attention of scholars because of its potential to reduce aircraft pollution and mitigate greenhouse gas emissions. A direct one-step conversion of glyceride-based oil into HRJ over NiAg supported on SAPO-11 zeolite was investigated in this paper. Also, the properties of the catalysts were characterized using XRD, TEM, N₂ adsorption-desorption, TG and Py-FTIR. The NiAg/SAPO-11 catalyst showed good performance in terms of hydro-processing, hydro-cracking, and hydro-isomerization reactions with the assistance of citric acid (CA) and phosphotungstic acid hydrate (HPW). The key to high conversion, high selectivity, and high iso-alkane content depended mostly on the reaction temperature, metal dispersion, acid content and the pore structures of the zeolite. Furthermore, the fuel properties were tested in a GC-MS/FID and flash point tester to ensure to meet the ASTM D7655 specifications. Under the optimal reaction conditions, a conversion of 100%, selectivity of 84%, an I-to-N ratio of 2.1, a yield of 72%, an aromatics content of 7%, and a flash point of 58 °C were obtained. The mass, carbon and energy yield for both one-step and two-step processes were also determined. This study provides a novel technique for producing renewable jet fuel with higher production yield.

1. Introduction

In recent decades, there has been a growing interest in greenhouse gas emissions, such as CO₂, NO_x, CH₄, and SO_x, which are considered to be responsible for climate change. In the transportation sector, with the increasing demand for fuel, it has been estimated that 2–6% of global carbon emissions can be attributed to commercial aviation [1]. Around five million barrels of aviation jet fuel are consumed per day, accounting for 5.8% of total fuel consumption [2]. One-fifth of total available fuel is consumed for land and air transportation [3], and consumption will increase in the range of 80%–130% in the next decades, leading to a growth in CO₂ emissions from 16% to 79% [4]. Therefore, it is important to develop a proper alternative fuel to reduce CO₂ emissions. The International Air Transport Association (IATA) made a commitment to achieve carbon-neutral growth in 2009: (1) an average annual improvement in fuel efficiency of 1.5% from 2010 to 2020, (2) carbon-neutral growth from 2020 onwards, and (3) a reduction in carbon emissions of 50% by 2050 compared to 2005 [5]. The International Energy Agency has estimated that up to 27% of total transport fuel could be provided by biofuels by 2050 [6]. Therefore, there is a need to develop a low pollution process that produces a sustainable fuel and reduced the emissions from aircraft engines.

Alternative jet fuels can be divided into two categories: synthetic fuels and renewable fuels [7]. Through the Fischer-Tropsch (F-T) process, synthesized gases such as carbon monoxide and hydrogen derived from coal and natural gas are liquefied to synthetic jet fuels [8]. On the other hand, renewable jet fuels can be produced from biomass such as plant oils and animal fats through hydro-conversion and are thus termed hydro-processed renewable jet (HRJ) fuel. In the literature studied, glyceride-based oil has been applied for producing HRJ fuel. As an economically important feedstock traded worldwide, palm oil derived renewable fuels have been received significant attentions. The global production of palm oil was around 72.27 million metric tons in the year of 2019/2020 [9]. Besides, the chain length of fatty acids composted in palm oil make it suitable as an alternative fuel with high cetane number and heating value after hydro-conversion [10,11]. Li et al. [12] reported the production of jet biofuel with 11% arene and 65% alkanes using zeolite catalyst. The refined bleached deodorized palm oil and palm kernel oil have also been used for producing bio-hydrogenated kerosene [11]. The previous studies have proved that palm oil can serve as a suitable feedstock for producing renewable jet fuel.

HRJ fuel can be produced using a two-step process including hydro-processing (hydro-deoxygenation, decarboxylation and decarbonylation), hydro-cracking, and hydro-isomerization over bi-functional catalysts. The hydro-processing reaction is the first step, where

* Corresponding author.

E-mail address: wilsonwang@mail.ncku.edu.tw (W.-C. Wang).

Nomenclature

<i>M</i>	Molar quantities of triglycerides (mol)
<i>N</i>	Molar quantities of product (mol)
<i>A</i>	Carbon atom number of product
Δm	Mass of palm oil feedstock (gram)
<i>m</i>	Mass (gram)
<i>C</i>	Mole of carbon (mole)
<i>E</i>	Energy (Joule)
<i>Q</i>	Energy input to the reactor (Joule)

Subscripts

<i>TO</i>	Total palm oil
<i>TG</i>	Palm oil after reaction
<i>TH</i>	C_8-C_{16}
<i>i</i>	Species i
<i>I</i>	Iso-alkanes
<i>N</i>	Normal alkanes
<i>A</i>	Aromatics
<i>p</i>	Product
<i>H</i>	Hydrogen
<i>c</i>	Coke
<i>G</i>	Gas
<i>F</i>	Feedstock

Abbreviations

HRJ	Renewable jet fuel
CA	Citric acid
HPW	Phosphotungstic acid hydrate
IATA	International Air Transport Association
F-T	Fischer-Tropsch
SAPO-11	Silicoaluminophosphates-11
GC	Gas chromatograph
MS	Mass spectrometer
FID	Flame ionization detector
wCA	Without citric acid
wHPW	Without phosphotungstic acid hydrate
MFC	Mass flow controller
BPR	Back pressure regulator
LHSV	Liquid hourly space velocity
XRD	X-ray diffraction
TEM	Transmission electron microscopy
BET	Brunauer, Emmett and Teller
BJH	Barret, Joyner and Halenda
TG	Thermogravimetric
FAME	Fatty acid methyl ester
Py-FTIR	pyridine adsorbed Fourier transform infrared spectrometer

vegetable oils or animal fats are converted into hydrocarbons over a sulfide NiMo/ γ -Al₂O₃, NiW/Al₂O₃, or CoMo/Al₂O₃ catalyst [13–15]. The next step is the combination of hydro-cracking and hydro-isomerization, where hydrocarbons in the jet fuel range can be obtained. Liu et al. [16] studied the hydro-conversion of castor oil over Ni-based catalysts in the second step and showed that the catalytic activity was associated with the mole ratio of the metal and the various acid strengths of the zeolites. A bi-functional catalyst consists of metal and zeolite, which are mainly responsible for the hydrogenation of unsaturated triglyceride and the degree of hydro-cracking, respectively [17]. A proper bi-functional catalyst for hydro-isomerization has shape-selectivity with regard to producing enough isomers and also reducing by-products [18]. Metals supported on silicoaluminophosphates-11 (SAPO-11) show acceptable performance on the hydro-isomerization of long n-alkanes [19,20], owing to their suitable acidity and pore structure. Due to its hierarchical porosity and moderate acidity, this mesoporous zeolite is promising for the application to catalytic conversion of bulky substrates. In general, HRJ fuel produced from the two-step process referred to above has good properties, including a low freezing point, a high octane number, and a high heating value. As mentioned above, catalysts used for hydro-processing are mainly in the form of sulfides. To maintain activity, the addition of sulfur-containing compounds such as H₂S or dimethyl disulphide is necessary. However, the use of these sulphiding agents causes the formation of undesirable S containing in HRJ, H₂S emission, and corrosion problems [21]. A one-step process using non-sulfided noble metals supported on SAPO-11 can solve the above problems. However, due to high hydrogenation of noble metals, isomeric products can be converted into light alkanes due to cracking [22,23], which in turn, results in a low yield of renewable jet fuel.

There are some advantages to a one-step process, such as shortening the process scheme, simplifying the operation, and reducing hydrogen and energy consumption. Wang et al. [24] investigated hydro-conversion of soybean oil over Pt/SAPO-11 and found that the deoxygenation via decarboxylation/decarbonylation of oils was favored at high temperatures, low pressure, and a low H₂/oil ratio. The major problem encountered is the presence of water in the zeolite framework [25], which poisons noble metals. The high cost of using noble metals

also makes application on a large scale infeasible. Liu et al. [26] indicated catalysts with 7 wt% Ni supported on modified SAPO-11 and achieved a high liquid alkane yield of 70%. In cases where noble metals are not used, a one-step process over transition metals is still available.

Both synthetic fuels and renewable fuels must be approved by ASTM D7566 [27], which is an expansion of D1655 to ensure that fuels blended with traditional jet fuel are certified. Several properties for jet fuels have been specified, including the flash point, freezing point, and aromatics content. The flash and freezing point effects are used to ensure that the fuel is free from fire hazardous and that it maintains flow at high altitudes, respectively. In terms of the aromatics content, fuels derived from F-T process are mainly composed of highly branched paraffins with a small amount of n-paraffins and cycloparaffins [28]. For the jet fuels derived from glyceride-based oils, the aromatics content depends on the types of feedstocks. When there is more linoleic or linolenic acid content in the feedstocks, more aromatics can be produced during hydro-conversion [29]. Without the aromatics composition, neat paraffinic-type fuels will cause O-ring seals to shrink, harden, and fail [30]. However, compared to paraffins, aromatics have a higher sooting tendency, which leads to erosion of turbine blades [31]. ASTM D7566 specifies that the aromatics content needs to be between 8 and 25 vol % for fuel blending.

Currently, little research has been conducted for the purpose of developing one-step HRJ production with the fuel obtaining a high mass yield. This work focused on the hydro-conversion of the glyceride-based oil into HRJ fuel. Palm oil was chosen as the feedstock due to its availability in Asia [32]. In addition, palm oil was selected as the glyceride-based oil in this study because triglyceride is the majority in palm oil. The products produced through both one-step and two-step processes over Ni-based catalysts were compared. In addition, Ni-based catalysts were prepared using different metals and various loadings with auxiliary agents. The objective of this work was to determine the influences of these loadings and investigate the reaction pathways. Based on the product analysis, the fuel properties could be studied based on their composition.

2. Experimental procedure

2.1. Materials

2.1.1. Palm oil composition

The palm oil used for hydro-conversion was provided by Meifeng Chemical Co., Ltd. The composition of the palm oil was analyzed using a gas chromatograph (GC) equipped with a mass spectrometer (MS) and a flame ionization detector (FID). The testing method is described in the next section. Before the GC tests, the palm oil has to be pre-treated through a transesterification method using an acid catalyst [33], for which the volume ratio of methanol, palm oil, and sulfuric acid were 2:3:0.5. They were mixed in a glass bottle and heated at 70 °C overnight (12 h). After the reaction, the liquid was separated using a separatory funnel, and hexane and saturated saline were added to extract the oil and water phases. Due to the lower density of the oil, the upper liquid was selected, and the hexane in the liquid was dried out with nitrogen. The resulting methyl esters were diluted with hexane and then analyzed on the GC-MS/FID. The composition of the palm oil is provided in Table 1.

2.1.2. Catalyst preparation

Nickel nitrate hexahydrate, $\text{Ni}(\text{NO}_3)_2 \cdot 6\text{H}_2\text{O}$ ($\geq 98.0\%$ analytical standard) was purchased from Alfa Aesar Co., Ltd. Silver nitrate, AgNO_3 was purchased from Honeywell Fluka Co. Citric acid, $\text{C}_6\text{H}_8\text{O}_7$ ($\geq 99.5\%$ analytical standard) was purchased from Sigma Aldrich Co. Phosphotungstic acid hydrate, $\text{H}_3\text{PW}_{12}\text{O}_{40} \cdot x\text{H}_2\text{O}$ ($\geq 99.0\%$ analytical standard) was purchased from Vetec Quimica Fina Ltd., and silicoaluminophosphates-11, SAPO-11 ($\text{Si}/\text{Al} = 0.4$) was provided by A-plus Inc.

NiAg/SAPO-11 catalysts with an Ni loading of 30 wt% were prepared via the wetness impregnation method [35]. Citric acid (CA) and phosphotungstic acid hydrate (HPW) were used as auxiliary agents to promote the dispersion of Ni particles [36] and the density of acid sites for isomerization [37,38], respectively. Nickel nitrate hexahydrate, citric acid (CA/Ni molar ratio = 1.5), and phosphotungstic acid hydrate (loading of 4 wt%) were first dissolved in 20 ml of deionized water. Then, SAPO-11 was added into the suspension and was continuously stirred at 70 °C for 5 h. After that, the mixture was dried in an oven at 180 °C overnight and then calcined in air at 500 °C for 5 h.

Ag is inactive in a high-temperature atmosphere [39]; therefore, it is inappropriate for use in calcination. Therefore, an alternative wetness impregnation method was performed. After calcination, the obtained powder precursors were dissolved in 10 ml of deionized water. Then, silver nitrate (Ni/Ag molar ratio = 44) was added into the suspension, followed by the same stirring and drying steps mentioned above.

NiAg/SAPO-11 catalysts were prepared with different Ni, CA, and HPW loadings, including Ni loadings of 20%, 25%, and 30% (CA/Ni molar ratio = 1.5 and 4 wt% HPW were the same individually) [16]. These are referred to x% NiAg/SAPO-11 , where x is the loading percentage of Ni. The 30% NiAg/SAPO-11 without adding citric acid or phosphotungstic acid hydrate are referred to 30% NiAg/SAPO-11 (wCA) and 30% NiAg/SAPO-11 (wHPW), respectively. Another one is referred

Table 1
The compositions of the palm oil.

Fatty acid	Abbreviation	Formula	Composition (mol %)
Myristic acid	C _{14:0}	C ₁₄ H ₂₈ O ₂	0.67
Palmitic acid	C _{16:0}	C ₁₆ H ₃₂ O ₂	39.60
Stearic acid	C _{18:0}	C ₁₈ H ₃₆ O ₂	9.40
Oleic acid	C _{18:1}	C ₁₈ H ₃₄ O ₂	40.22
Linoleic acid	C _{18:2}	C ₁₈ H ₃₂ O ₂	9.27
Undetected fatty acid [34]	(C _{12:0} ; C _{18:3} ; C _{20:0})	C ₁₂ H ₂₄ O ₂ C ₁₈ H ₃₀ O ₂ C ₂₀ H ₄₀ O ₂	0.84

to 30% NiAg/SAPO-11 (wCA and wHPW).

2.2. Experimental setup

The reactions (hydro-processing, hydro-cracking, and hydro-isomerization) were all carried out in a fixed bed continuous flow system, as shown in Fig. 1. According to the different requirements, the SUS316L tubes were varied in diameter, including 13, 6, and 3 mm. The purity of the hydrogen and nitrogen were 99.999% and 99.99%, respectively. For the purpose of hydro-conversion, hydrogen was introduced into the system using a mass flow controller (MFC, 5850i, Brooks, USA). Nitrogen was introduced into the system manually for the purpose of the leak test. Palm oil as the feedstock was fed into the system using a high pressure pump (SN-26158, Eldex, USA). Before being fed into the system, a hot plate stirrer (AL-HTS1003, LMS, Japan) was used to heat the palm oil in order to decrease its viscosity. The feedstock inlet line was pre-heated using heat tapes at half of the reaction temperature for preventing the reaction from cold-feeding and ensuring that the drop in temperature would not be significant. The fixed bed reactor was also made of SUS316L with an inside diameter of 12.7 mm and a length of 300 mm. To measure the reaction temperature, three K-type thermocouples were installed in the pre-heater as well as the inside and outside of the reactor. The system pressure was controlled through a back pressure regulator (BPR) installed downstream the reactor. A swirling copper tube with a length of 3800 mm was used to condense the gas product flowing out of the reactor. The product after condensation was flowed through a gas-liquid separator, which the liquid product was dripped down, and the gas product was floated up within the buffer tank.

For the purpose of achieving the required flash point, the produced fuel must be distilled to remove the short-chain hydrocarbons, which do not meet the flash point specifications. The produced fuel was heated and stirred using a heating mantle (MNS-500, New Lab, Taiwan) from room temperature to 180 °C, at which time the short-chain hydrocarbons began to vaporize. The instant temperature was observed to be in the range of room temperature to 360 °C, as shown in Fig. 2. In addition, the temperature at different selected distillate volume fractions was recorded to draw the distillation curve [40]. After distillation, the flash point of the fuel was examined using a Pensky Martens flash tester (NPM 131, Normalab, France). The sample was cooled down from the room temperature by 10 °C as a pretreatment, and a flame was applied every 1 °C until the sample ignited [41].

2.3. Reaction procedure

2.3.1. Reduction conditions

Once the catalysts were calcined, the next step is the reduction. Five grams of NiAg/SAPO-11 catalyst powder mixed with 1.5 g of SiC (purchased from Alfa Aesar) was packed in the center of the reactor. SiC was used to minimize the axial temperature gradients and improve flow [42]. In order to prevent the catalyst from flowing out of the reactor, glass wool was used to plug the top and bottom of the reactor. After the catalyst packing was done, nitrogen was introduced into the system until the reaction pressure necessary to detect leaks was obtained. The heater was set at a specific temperature, and hydrogen was introduced into the system to reduce the catalyst at a flow rate of 50 sccm for 2 h.

2.3.2. Hydro-conversion

A hot plate stirrer was used to heat the palm oil at 70 °C before being fed into the system. The pre-heating section was set at 200 °C, which was half of the reaction temperature. The next step was to increase the hydrogen flow rate up to 100 sccm and to pump the palm oil into the system at a specific flow rate. At approximately 2 h later, the liquid product flowed out of the reactor and was cooled down together with the gas product using a condenser. The liquid product was collected after pressure release using a metering valve and the gas product was

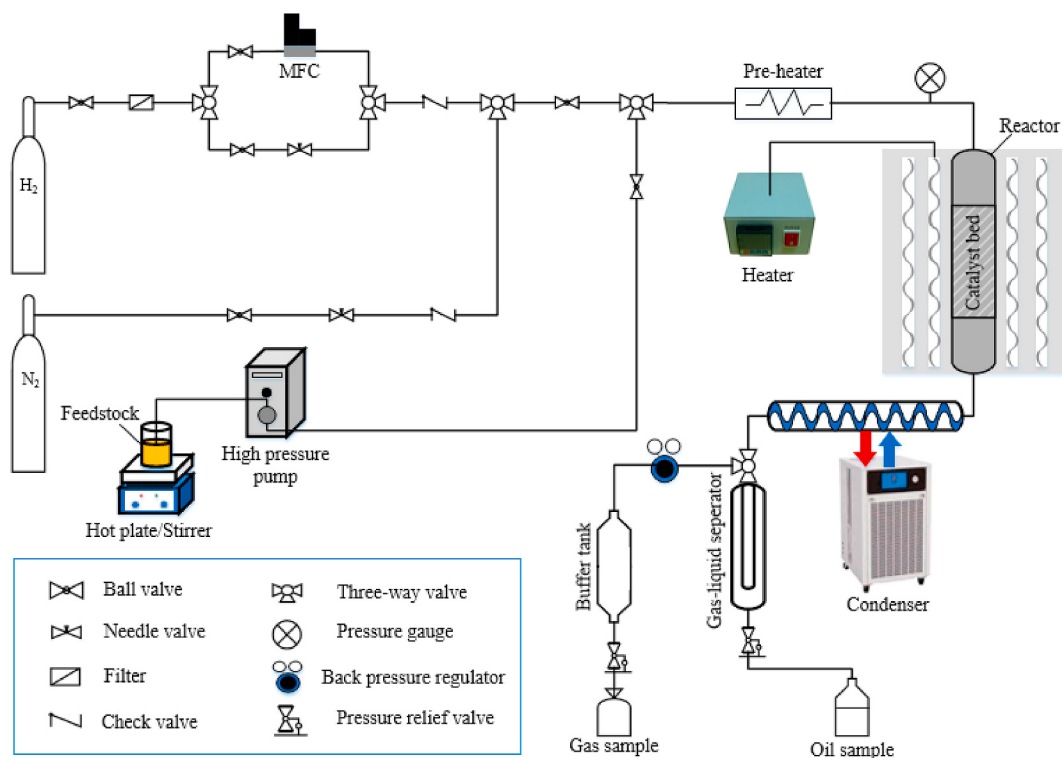
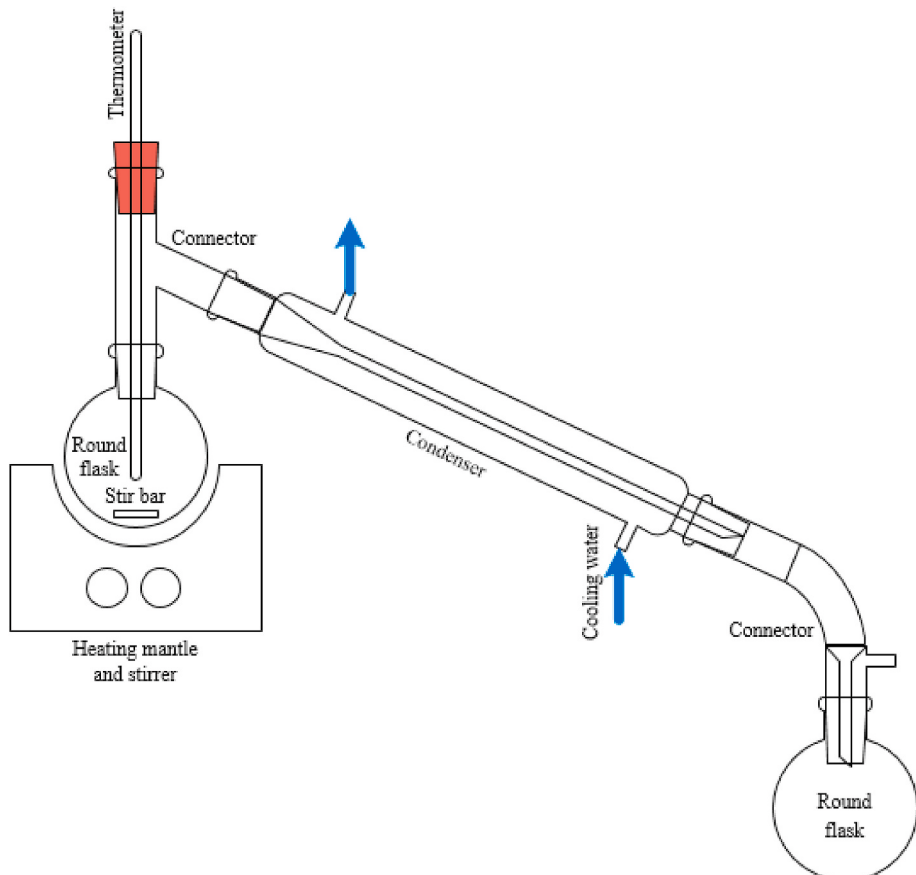
**Fig. 1.** Experimental setup.**Fig. 2.** Distillation system.

Table 2
Reaction conditions for catalyst reduction and hydro-conversion.

Condition	Reduction	Hydro-conversion
Temperature (°C)	400	380–420
Pressure (bar)	52	38–59
H ₂ flow rate (sccm)	50	100
LHSV (h ⁻¹)	N/A	0.5–2

collected after pressure release using a metering valve into the sampling bags. The reduction and hydro-conversion conditions are provided in Table 2. Liquid hourly space velocity (LHSV) is defined as the ratio of the liquid volume flow per hour to the catalyst volume, which is inversely proportional to the residence time. Different LHSV values were obtained by adjusting the feeding flow rate as well as H₂ flow rate in order to maintain the H₂/oil ratio.

2.4. Catalyst characterization

2.4.1. X-ray diffraction

X-ray diffraction (XRD) was used to determine the crystal and pore structure of the catalysts. The powder patterns of the catalysts were recorded on a Shimadzu XRD 7000S diffractometer (Shimadzu, Japan), with CuK α radiation ($\lambda = 1.5406 \text{ \AA}$) at 30 kV, 30 mA and a scanning rate of 3°/min in a 2 θ range of 10–80 °C.

2.4.2. Transmission electron microscopy

Transmission electron microscopy (TEM) was used to characterize the surface morphology of the specimens. The specimens were prepared by depositing a drop of an ethanol suspension of the solid catalysts on carbon coated Cu grids. TEM was carried out on a Hitachi H-7500 (Hitachi, Japan), with an accelerating voltage of 80 kV.

2.4.3. Textural properties

Textural properties, including surface area, pore volume, and pore size, were acquired with N₂ adsorption/desorption isotherm measurements at –196 °C on a Micromeritics TriStar II 3020 (Micromeritics, USA). BET was used as the surface area calculation method (Brunauer, Emmett and Teller), and the pore volume and pore size were calculated using the BJH (Barret, Joyner and Halenda) method.

2.4.4. Thermogravimetric analysis

A thermogravimetric (TG) analysis of the spent 30% NiAg/SAPO-11 catalyst was carried out on a TA-Q50 analyzer (TA Instruments, USA). About 40 mg of the catalyst sample was placed into a platinum crucible and heated from 100 °C to 800 °C at a rate of 10 °C/min. A dry air flow rate of 60 ml/min was set to remove the gases decomposing out of the catalyst.

2.4.5. Pyridine adsorbed Fourier transform infrared spectrometer

A pyridine adsorbed Fourier transform infrared spectrometer (Py-FTIR) was used to measure the content of the Lewis and Brønsted acid sites. The spectra were recorded on a Nicolet iS5 FTIR spectrophotometer (Thermo Scientific, USA) to evaluate the catalyst with pyridine chemically adsorbed in an infrared range of 1400–1600 cm^{−1} [43].

2.5. Lipid and product analysis

2.5.1. Palm oil

Qualitative and quantitative analyses were conducted in GC-MS and GC-FID, respectively. The palm oil was analyzed in the form of a free fatty acid methyl ester (FAME) after transesterification. A total of 85 μ L of the methyl ester sample was diluted with 5 ml hexane (HPLC grade, Fisher Scientific) and injected into a GC by 1 μ L at 280 °C. The GC-MS/FID analysis of the lipid was carried out on a Shimadzu QP2010 instrument equipped with the same capillary columns. The capillary

columns were HT-5 (SGE, 30 m × 0.25 mm × 0.1 μ m) with a helium carrier gas set at a constant flow rate of 1 ml/min. The oven temperature varied with time: the initial temperature was 120 °C, which was held for 3 min and then ramped 15 °C/min to 200 °C, held for 0.5 min and then ramped 5 °C/min to a final temperature 280 °C and held for 5 min.

2.5.2. The analysis of liquid and gas products

The same ratio of diluted renewable jet fuel sample was injected into the GC by 1 μ L at 200 °C. The capillary columns were HT-5 (SGE, 30 m × 0.25 mm × 0.1 μ m) with the helium carrier gas set at a constant flow rate of 2 ml/min. The oven temperature profile was as follows: an initial temperature of 35 °C, which was held for 1 min, ramped 1 °C/min to 40 °C, held for 0 min, ramped 12 °C/min to 196 °C, held for 3 min, and ramped 5 °C/min to a final temperature of 200 °C and held for 5 min.

0.2 ml of the organic gas sample was directly injected into the GC at 200 °C. The helium carrier gas was set at a constant flow rate of 2 ml/min. The temperature gradient was as follows: an initial temperature of 35 °C, held for 1 min and ramped 1 °C/min to the final temperature of 43 °C. The inorganic gas samples, such as CO and CO₂, were investigated using a gas chromatography-thermal conductivity detector (GC-TCD, GC2014AT, Shimadzu) equipped with a TDX-01 (3 m × 3 mm) packed column, and helium was used as the carrier gas. The temperature of 80 °C was maintained for 23 min.

2.5.3. Calculation methods

The products were composed of mainly normal and iso alkanes with a small amount of cyclic hydrocarbons and aromatics. The quantitative analysis was calibrated using C₈–C₂₀ normal alkanes as the external standard, in accordance with the composition in the final product. The following equations provide relevant definitions:

$$\text{Conversion } (\%) = \frac{M_{TO} - M_{TG}}{M_{TO}} \times 100\%, \quad (1)$$

where M_{TO} and M_{TG} are the molar quantities of total palm oil and the palm oil after the reaction, respectively.

$$\text{Selectivity } (\%) = \frac{M_{TH}}{\sum_i^i N_i \times A_i} \times 100\%, \quad (2)$$

where M_{TH} is the total molar quantities of the C₈–C₁₆ hydrocarbons; N_i is the molar quantities of product i , and A_i represents the carbon atom number of product i .

$$\text{I-to-N ratio} = \frac{M_I}{M_N}, \quad (3)$$

where M_I is the total molar quantities of iso-alkanes, and M_N represents the total molar quantities of normal alkanes in the product.

$$\text{Aromatics } (\%) = \frac{M_A}{\sum_i^i N_i \times A_i} \times 100\%, \quad (4)$$

where M_A is the total molar quantities of aromatics; N_i is the molar quantities of product i , and A_i represents the carbon atom number of product i .

$$\text{Yield } (\%) = \frac{m_p}{\Delta m} \times 100\%, \quad (5)$$

where Δm is the weight of the palm oil fed into the system, and m_p represents the weight of the product.

3. Results and discussion

3.1. Catalyst characterization

3.1.1. X-ray diffraction

NiAg/SAPO-11 catalysts with citric acid added (CA/Ni molar ratio =

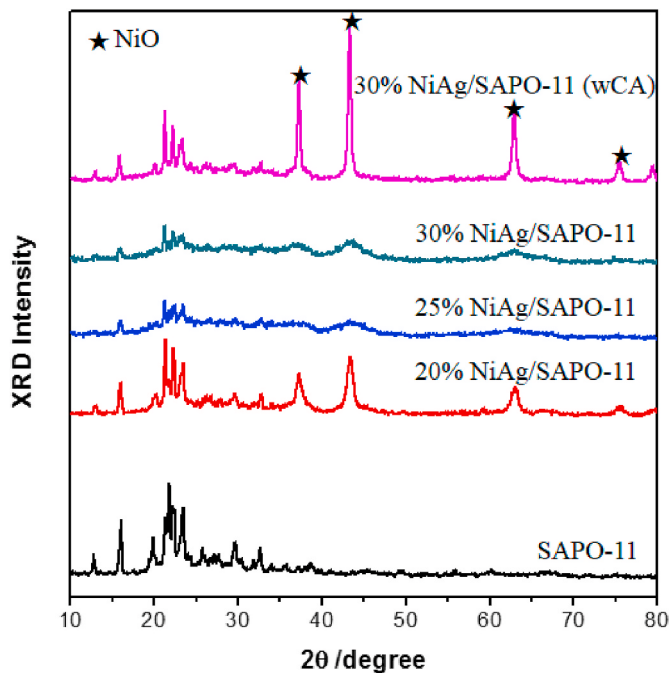


Fig. 3. NiAg/SAPO-11 XRD patterns.

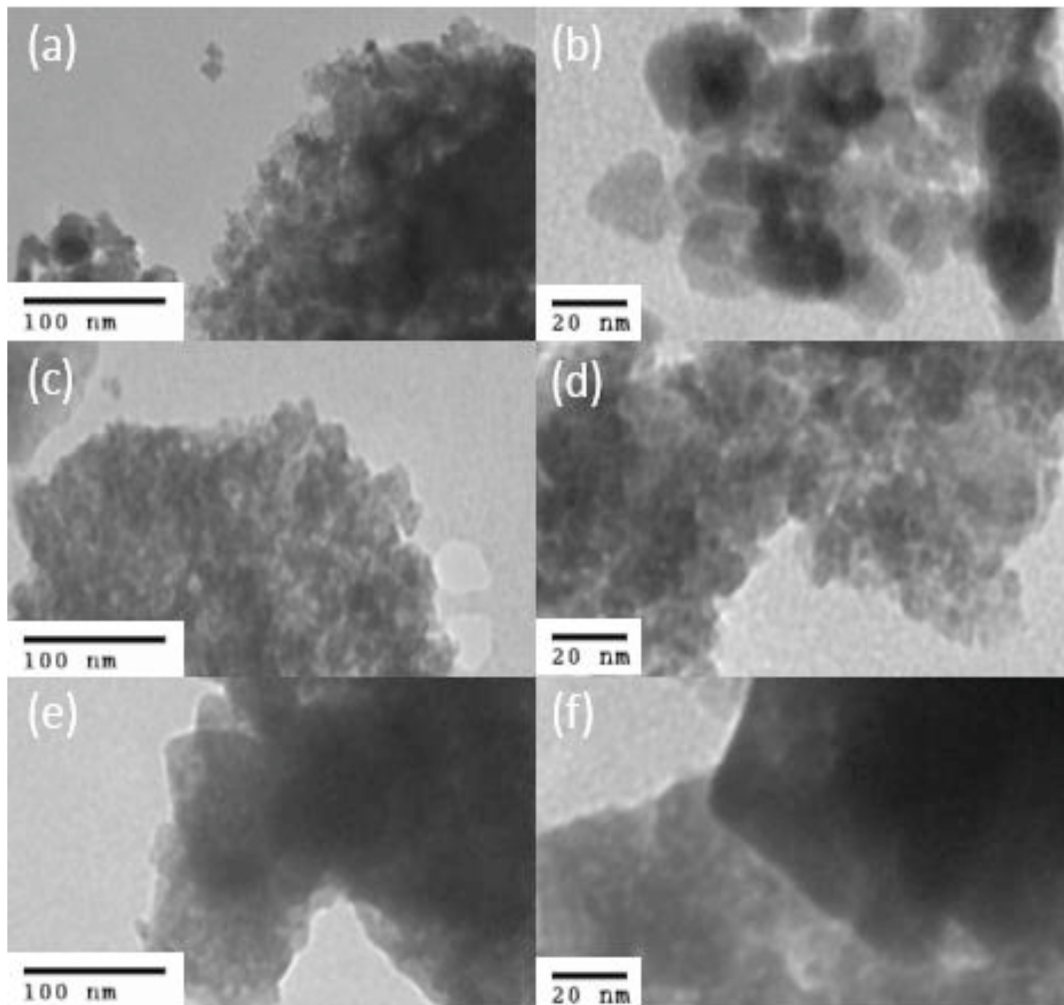


Fig. 4. TEM images of 20% NiAg/SAPO-11 (a, b), 30% NiAg/SAPO-11 (c, d) and 30% NiAg/SAPO-11 (wCA) (e, f).

1.5) were synthesized with different Ni loadings, for which the XRD patterns are shown in Fig. 3. Compared with pure SAPO-11, the diffraction patterns of the synthesized catalysts indicated that their structures were consistent with the AEL-type in phase at $2\theta = 13^\circ$ to 23° . For the same Ni loading of 30%, the samples with citric acid added had small peaks in phase at $2\theta = 37^\circ$, 43° , 63° , and 76° corresponding to the NiO crystallites. This proved that citric acid helped Ni disperse better and led to decreased particle sizes. However, the diffraction peaks of the 20% NiAg/SAPO-11 were bigger than those of the 25% and 30% catalysts, indicating the aggregation of NiO crystallites. It might have been due to the lack of citric acid content. As a chelating ligand, citric acid has been found to play an important role in improving Ni dispersion [44].

3.1.2. Transmission electron microscopy (TEM)

The TEM images showed the Ni distribution surface morphology, as shown in Fig. 4. Obviously, with the exception of the images of 30% NiAg/SAPO-11 (Fig. 4c and d), the other images revealed that there were many agglomerations of Ni clusters. The TEM results were in accordance with the XRD pattern because the 30% NiAg/SAPO-11 indeed had smaller particle sizes, and the Ni dispersion was better than that of the 20% NiAg/SAPO-11 (Fig. 4a and b) and the 30% NiAg/SAPO-11 (wCA) (Fig. 4e and f). With high active metal dispersion, the reaction of hydro-conversion will thus be improved, resulting in high conversion and selectivity [45].

Table 3
Textural properties of the NiAg/SAPO-11 catalysts.

Catalyst	Surface area ^a (m ² g ⁻¹)	Pore volume ^b (cm ³ g ⁻¹)	Pore size ^b (nm)
SAPO-11	73.2	0.258	12.3
20% NiAg/SAPO-11	50.7	0.178	10.8
25% NiAg/SAPO-11	56.9	0.116	5.1
30% NiAg/SAPO-11	72.8	0.157	5.8
30% NiAg/SAPO-11 (wCA)	31.7	0.146	11.3

^a Calculated by BET method.

^b Calculated by BJH desorption method.

3.1.3. Textural properties

The surface area, pore volume, and pore size are presented in Table 3. The molecular sieve of SAPO-11 can be divided into micropores and mesopores, which are composed of ten-membered rings of 0.4 nm × 0.65 nm and their stacking particles, respectively [46]. Comparing the surface area and pore volume of SAPO-11 with those of the catalyst, an apparent drop was observed. This was due to the blocked microchannels, resulting from large Ni particles. However, with the assistance of citric acid, the 30% NiAg/SAPO-11 still had a similar surface area to that of SAPO-11, owing to the smaller Ni particle sizes. Citric acid simultaneously caused the pore volume to increase but the high loading of Ni caused it to decrease. Fortunately, the pore volume of the 30% NiAg/SAPO-11 was large enough to cause the reaction. The 25% and 30% NiAg/SAPO-11 had excellent hydro-conversion performance despite the small pore sizes. The diameter of triglyceride is only around 0.6 nm, so a pore size of 5 nm is big enough for feedstocks. It is possible that the nano-sized Ni crystallites entered the microchannels of SAPO-11, providing high activity for small hydrocarbons. According to this result, the changed pore sizes were in accordance with the low intensities of the AEL-type crystal structure of SAPO-11.

3.1.4. Thermogravimetric analysis (TGA)

The TG profile of the spent catalyst was used to study the coke deposition after the experiment, as shown in Fig. 5. In general, weight loss percentage can be investigated in three different temperature regions ($T < 180$ °C, $180^{\circ}\text{C} < T < 330$ °C, and $T > 330$ °C) [47]. In region $T < 180$ °C, the significant weight loss was attributed to the desorption of water and some volatile species. In the $180^{\circ}\text{C} < T < 330$ °C and $T > 330$ °C regions, the loss was attributed to the formation of CO or CO_2 , resulting

from the decomposition of coke. A slight weight gain was observed at 350 °C, indicating that Ni began to be oxidized in the air flow. With the formation of oxidized Ni and the decomposition of coke, the derivative of the TG curve (the blue curve) was unsteady at temperatures over 500 °C. By calculating the weight loss, the coke deposition of the spent 30% NiAg/SAPO-11 was 7.5% (average value in triple runs) at temperatures ranging from 180 °C to 800 °C.

3.1.5. Pyridine adsorbed Fourier transform infrared spectrometer (Py-FTIR)

The Py-FTIR spectra revealed the distribution of the Brønsted and Lewis acid sites in the bands at 1540 cm⁻¹ and 1450 cm⁻¹, respectively, where 1490 cm⁻¹ was related to both the Brønsted and the Lewis acid [48]. As shown in Fig. 6, the spectra of the 30% NiAg/SAPO-11 (wCA and wHPW) showed low intensities of both acids. This was possibly due to the high loading concentration of Ni on the acid surface. On the other hand, high-intensity spectra appeared at 1450 cm⁻¹ and 1490 cm⁻¹, indicating that the amount of both acids increased with the assistance of CA and HPW. The reason for increasing the Lewis acid was the extra-framework aluminum, which was formed by CA removing Al from the framework [49]. For the spectra at 1540 cm⁻¹, there was no obvious peak. However, in spite of being short of Brønsted acid at 1540 cm⁻¹, the Brønsted acid might have been improved at 1490 cm⁻¹ by HPW.

3.2. Catalytic performance

3.2.1. Influence of the metal loadings

In the case of hydro-conversion, olefins are formed by the dehydrogenation of alkanes on metal sites and then become carbenium ions as intermediates through protonation on acid sites. The carbenium ions can be either hydro-isomerized through the skeletal rearrangement or hydro-cracked through the β -scission on the acid sites. Both isomerized and cracked olefins are eventually hydrogenated to alkanes on metal sites [50]. The liquid product distributions of the different metals loading are listed in Table 4. All of the catalysts showed high conversion for palm oil, representing excellent hydrogenation. At different Ni loadings, the 30% NiAg/SAPO-11 catalyst had the highest conversion and selectivity. A comparison of the 30% NiAg/SAPO-11 with the 30% Ni/SAPO-11 showed a significant concentration drop of C₁₅–C₁₈ due to adding Ag, which is a strong oxidizer with a +0.8V standard reduction potential in water at 25 °C. Therefore, the long-chain fatty acids could be deoxygenated and cracked more easily. In a fuel cell, Ag can be used as cathode to facilitate the breaking of the O–O band [51]. This improves deoxygenation by reducing oxygen (O₂) to water (H₂O) according to the reactions below:

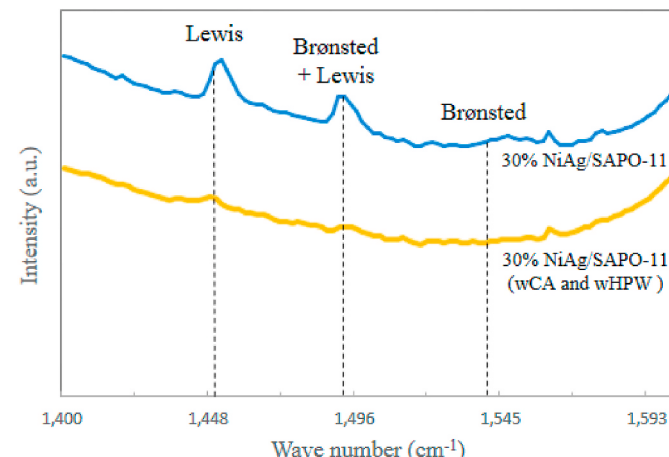


Fig. 6. Py-FTIR spectra of 30% NiAg/SAPO-11 and 30% NiAg/SAPO-11 (wCA and wHPW).

Table 4

Liquid product distribution of different metal loadings.

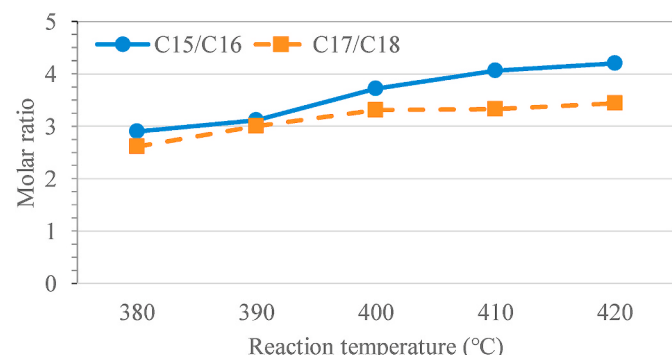
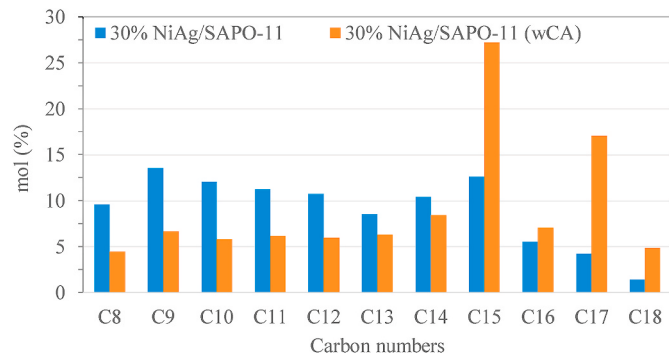
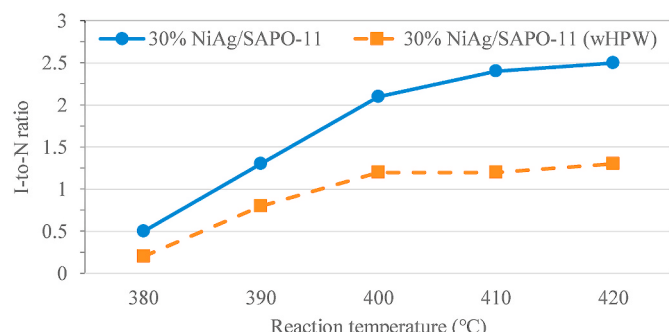
Catalyst ^a	Distribution (mol %)					
	C ₈ –C ₁₄		C ₁₅ –C ₁₈		Total	
	Iso alkanes ^c	Normal alkanes	Iso alkanes ^c	Normal alkanes	Conversion (%)	Selectivity ^d (%)
30% Ni/SAPO-11 ^b	20.0	24.6	13.0	42.4	100	72
20% NiAg/SAPO-11	7.5	14.2	19.0	59.3	95	61
25% NiAg/SAPO-11	29.0	28.4	13.7	28.9	98	80
30% NiAg/SAPO-11	53.9	22.5	15.4	8.2	100	84

^a Reaction conditions: T = 400 °C, P = 52 bar, H₂ flow rate = 100 sccm, LHSV = 1 h⁻¹.^b That is, 30% NiAg/SAPO-11 without adding Ag.^c Including aromatics and cyclic hydrocarbons for facilitated computation.^d Defined in the range of C₈–C₁₆ hydrocarbons.

However, in the presence of H₂O, NiO will be formed during the hydro-conversion. It may damage the stability of Ni and influence the hydrogenation performance. As a consequence, an approach involving decarbonylation plus decarboxylation is suggested. Palmitic acid (C_{16:0}) and oleic acid (C_{18:1}) are dominant in the composition of palm oil. The molar ratio of normal alkanes of C₁₅/C₁₆ and C₁₇/C₁₈ over the 30% NiAg/SAPO-11 at different temperatures shown in Fig. 7 was above 2.5, indicating that decarbonylation plus decarboxylation was dominant despite the addition of Ag.

3.2.2. Influence of the auxiliary agent loadings

Two auxiliary agents were applied in this study, including CA and HPW. The purpose of adding these compounds was to promote the Ni dispersion and acid density on SAPO-11, respectively. As shown in Fig. 8, the 30% NiAg/SAPO-11 catalyst showed a high distribution of alkanes (including isomeric and normal alkanes), resulting in selectivity a high as 84%. Although the selectivity of the 30% NiAg/SAPO-11 (wCA) was 78%, the high concentration of C₁₅–C₁₈ might have resulted in failing to meet the freezing point standard. With the assistance of CA, a larger surface area and smaller Ni particle sizes were obtained, which enhanced the formation of mesopores and improved isomerization. In general, Brønsted acid is responsible for cracking and isomerization; Lewis acid is for cracking and aromatization. As mentioned above, these two acid sites are both important for producing renewable jet fuel. HPW is a kind of heteropoly acid and provides high Brønsted acidity [52]. The I-to-N ratio of the 30% NiAg/SAPO-11 and the 30% NiAg/SAPO-11 (wHPW) at different temperatures was investigated, as shown in Fig. 9. The performance of the 30% NiAg/SAPO-11 on I-to-N ratio was always better than that without adding HPW. Regardless of the catalyst, the I-to-N ratio increased with increases in the temperature.

Fig. 7. Molar ratio of C₁₅/C₁₆ and C₁₇/C₁₈ over the 30% NiAg/SAPO-11.Fig. 8. Product distribution of the 30% NiAg/SAPO-11 and the 30% NiAg/SAPO-11 (wCA) (T = 400 °C, P = 52 bar, H₂ flow rate = 100 sccm, LHSV = 1 h⁻¹).Fig. 9. I-to-N ratio of the 30% NiAg/SAPO-11 and the 30% NiAg/SAPO-11 (wHPW). (P = 52 bar, H₂ flow rate = 100 sccm, LHSV = 1 h⁻¹).

When reaching a temperature of 400 °C, the I-to-N ratio of the 30% NiAg/SAPO-11 exceeded 2, where that of Jet A-1 was approximately 1.5. However, a balance between Brønsted and Lewis acids are of concern because C₆–C₈ olefins and propene attributed to the Brønsted acid site go through a Diels-Alder reaction at the Lewis acid site to form aromatics [53]. Each acid site plays an important role in the composition of the products. Thus, additional Brønsted acid sites for the one-step process are suggested.

3.2.3. Influence of the reaction conditions

Three variables, including the temperature, pressure, and LHSV, over the 30% NiAg/SAPO-11 are discussed in terms of their impact on HRJ. As shown in Fig. 10, a high conversion of palm oil was achieved at temperatures over 380 °C. In spite of the high conversion, the selectivity at 380 °C was only 70% (in the range of C₈–C₁₆), indicating that the temperature was not high enough to cause cracks in the long-chain hydrocarbons (C₁₇ and C₁₈). With the reaction temperature increased

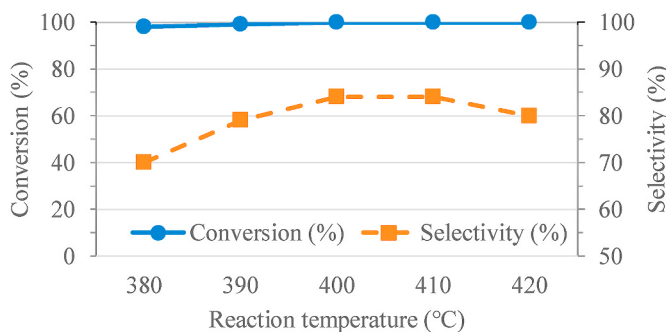


Fig. 10. Conversion and selectivity of the 30% NiAg/SAPO-11 at different temperatures. ($P = 52$ bar, H_2 flow rate = 100 sccm, LHSV = 1 h^{-1}).

to 400 °C, a selectivity of 84% was obtained. However, a drop of selectivity to 80% was observed due to more gas product produced due to severe cracking.

For the reaction pressure, both selectivity and the I-to-N ratio achieved their maximum at a pressure of 52 bar, as shown in Fig. 11. The high initial temperature and pressure improve the level of cracking while simultaneously enhance the hydrogen participating in the free-radical reaction. This suppresses the isomerization reaction [54]. Because iso-alkanes were generated by the combination of hydrocarbon free radicals, the enhanced hydrogen free radicals could be combined with hydrocarbon free radicals more easily. Because of this, the I-to-N ratio did not continue to increase when the pressure was raised to 52 bar.

As shown in Fig. 12, the selectivity decreased with increases in the LHSV, indicating that the lower hydro-conversion activity was due to the lower residence time of feedstock passing through the catalyst. Even though the LHSV increased to 2, the conversion of the palm oil was still maintained at high levels. Fig. 13 shows the selectivity increased with increases in the H_2 -to-oil ratio until 1000. The H_2 consumption for hydro-processing of glyceride-based oil into alkanes was elaborated in the authors' previous work [55]. More input of hydrogen would enhance the hydro-cracking reaction, which slightly reduces the selectivity. It can be seen that the selectivity between LHSVs of 1 h^{-1} and 0.5 h^{-1} has the difference of 4%. Applying LHSV of 1 h^{-1} results in higher scale of production. Therefore, LHSV of 1 h^{-1} was chosen as the optimal value.

3.2.4. Proposed reaction mechanism

The proposed reaction pathways for the one-step hydro-conversion are shown in Fig. 14. First, palm oil composed of unsaturated triglyceride was hydrogenated to saturated triglyceride by Ni at 200 °C. Then, oxygen atoms were removed by Ni via deoxygenation. There are three pathways for hydro-processing of a saturated triglyceride [56]. Normal alkanes with the same carbon number ($n\text{-RCH}_3$) as the fatty acid are produced by releasing H_2O via hydro-deoxygenation. Normal alkanes

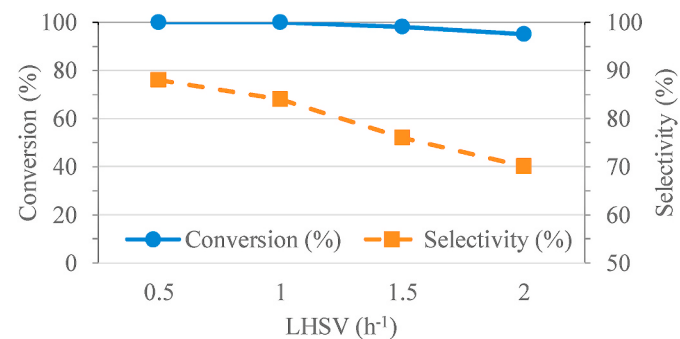


Fig. 12. Conversion and selectivity of 30% NiAg/SAPO-11 at different LHSV values. ($T = 400$ °C, $P = 52$ bar, H_2 flow rate = 100 sccm).

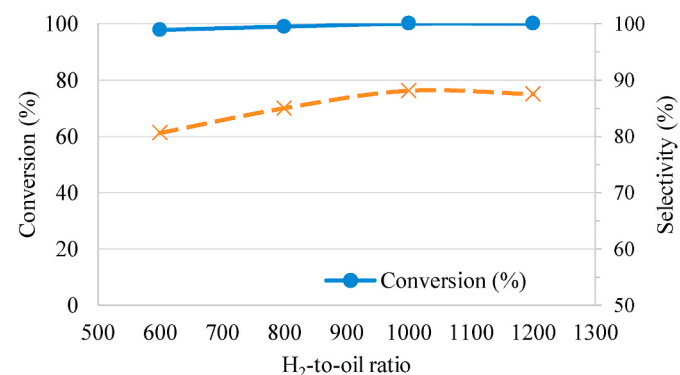


Fig. 13. Conversion and selectivity of 30% NiAg/SAPO-11 at different H_2 -to-oil ratios. ($T = 400$ °C, $P = 52$ bar, LHSV = 1 h^{-1}).

with one carbon less ($n\text{-RH}$) than the fatty acid are produced by releasing CO and CO_2 via decarbonylation and decarboxylation, respectively. All of these pathways generate C_3H_8 as a by-product, which can be dehydrogenated to C_3H_6 . After obtaining the normal alkanes, light alkanes are produced by the metal site (Ni) and acid sites (Brønsted and Lewis acids) via cracking. Iso-alkanes are produced from light alkanes or normal alkanes by Ni and the Brønsted acid site via isomerization. The compositions of cyclic hydrocarbons and aromatics depend on both the metal and Lewis acid sites. When $C_6\text{--}C_8$ olefins and C_3H_6 produced from the light alkanes undergo the Diels-Alder reaction, five-membered hydrocarbon rings take shape. In addition, the C_3H_8 produced from the hydrogenolysis of the saturated triglyceride dehydrogenated to C_3H_6 can also react with $C_6\text{--}C_8$ olefins via the Diels-Alder reaction. Eventually, some cyclic hydrocarbons are converted to aromatics by the Ni and Lewis acid sites via ring expansion.

3.3. Product analysis

3.3.1. Comparisons of GC-FID spectra

For the purpose of making comparisons of the products, the GC-FID spectrum of Jet A-1 (Fig. 15a) was taken as a reference. Between each normal alkane shown in Figs. 15 and 16 are mainly iso-alkanes as well as few cyclic hydrocarbons and aromatics. Comparing Figs. 15b and c for the one-step hydro-conversion, the spectrum of HRJ over the 30% NiAg/SAPO-11 ($T = 400$ °C, $P = 52$ bar, H_2 flow rate = 100 sccm, LHSV = 1 h^{-1}) was more similar to that of Jet A-1 than to that over the 1% Pt/SAPO-11 (provided by A-plus Inc., reaction conditions of $T = 450$ °C, $P = 59$ bar, H_2 flow rate = 100 sccm, and LHSV = 1 h^{-1}). Although the HRJ shown in Fig. 15c had good cold flow properties due to having lots of iso-alkanes, the lack of normal alkane content led to a low heating value. In addition, the $C_{15}\text{--}C_{18}$ content was almost completely removed because of a strong cracking reaction. Here, we also compared the HRJ

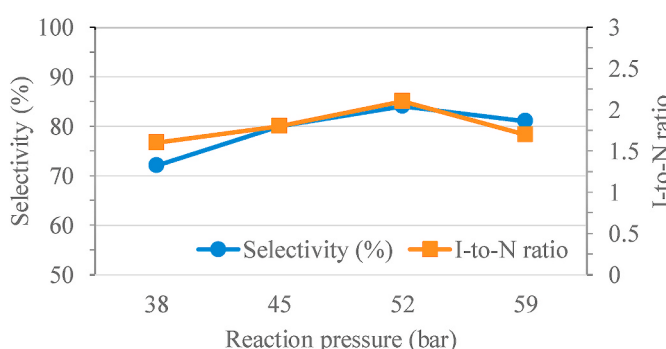


Fig. 11. Selectivity and I-to-N ratio of the 30% NiAg/SAPO-11 at different pressures. ($T = 400$ °C, H_2 flow rate = 100 sccm, LHSV = 1 h^{-1}).

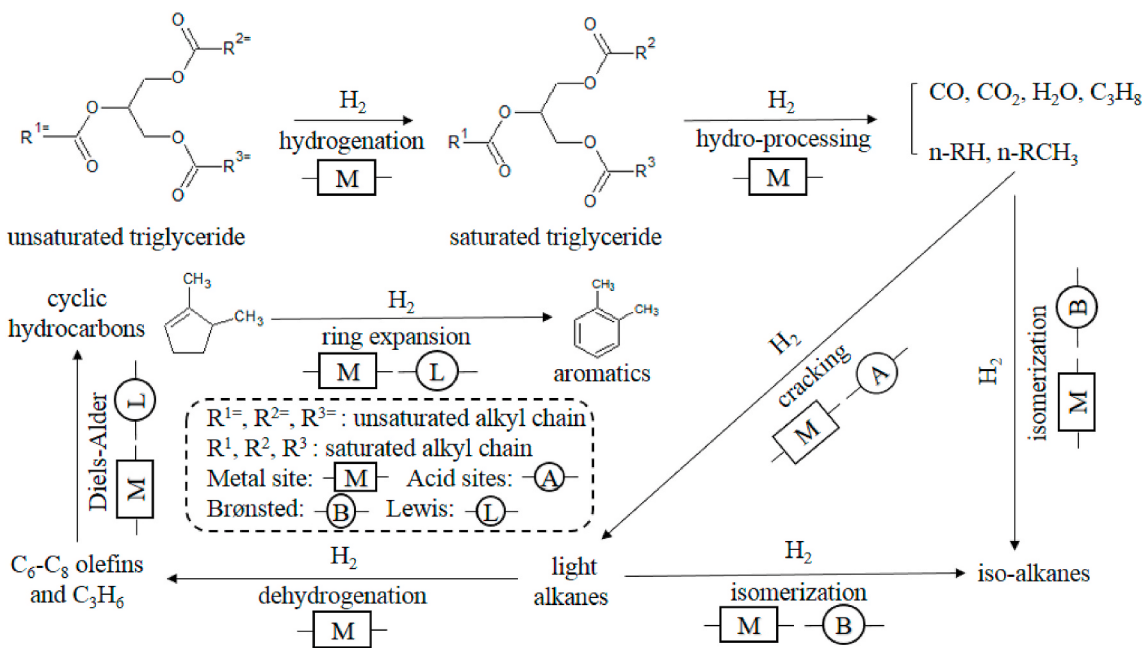


Fig. 14. Proposed reaction pathways for the one-step hydro-conversion.

from the two-step hydro-conversion, whose feedstock was hydro-processed alkanes converted from palm oil over NiMo/γAl₂O₃ (provided by A-plus Inc., reaction conditions of T = 400 °C, P = 47 bar, H₂ flow rate = 300 sccm, and LHSV = 3 h⁻¹). The hydro-processed alkanes comprised mainly normal alkanes in the range of C₈ to C₁₈, as shown in Fig. 16. The HRJ produced from the green diesel showed a good I-to-N ratio of 1.5. However, the high content of C₁₆ to C₁₈ might have caused the freezing point to fail to meet the standard requirement [57]. In general, flash point and freezing point failures are associated with the presence of short-chain hydrocarbons and long-chain hydrocarbons, respectively.

3.3.2. Properties and distillation characteristics of the renewable jet fuels

As shown in Table 5, the fuel properties, such as the aromatics content and the HRJ-1 flash points (from the one-step process) and the HRJ-2 flash points (from the two-step process) were obtained. Both fuels met the specification requiring the flash point to be over 38 °C and even exceeded the standard. It was discovered that the distillation curve had an impact on the flash point [58]. As shown in Fig. 17, the boiling points of HRJ-1 and HRJ-2 were approximately 200 °C, which were 20 °C higher than that of Jet A-1. The distillation curves of HRJ-1 and HRJ-2 are different due to the different composition distribution. In terms of the aromatics content, which requires 8% for the blended fuel (ASTM D7566), both HRJ-1 and HRJ-2 were acceptable. The yield in the one-step process after distillation was 72%, which was significantly better than the 50% obtained with the two-step process. In Fig. 18, it can be seen that the mole fraction values of CO plus CO₂ were all over 60% at each stream time. This proved that the deoxygenation pathway was mainly via decarbonylation and decarboxylation. On the other hand, little or no C₃H₈ was obtained in the gas product. It was possible that the C₃H₈ participated in the Diels-Alder reaction to form cyclic hydrocarbons and aromatics.

3.4. Mass, carbon and energy yields for the process

The mass yield before distillation was obtained from Eqn. (5), which refers to the ratio of the masses of the product and feedstock. The mass of gas (m_G) was calculated based on the conservation of mass,

$$m_H + \Delta m = m_P + m_G + m_C, \quad (9)$$

where m_H , Δm , m_P , m_G , and m_C are the mass of hydrogen, feedstock, product, gas, and coke, respectively. The mass of hydrogen was determined by calculating the minimum hydrogen consumption for converting palm oil into jet fuel. The mass of coke was estimated according to the results of the TG profile, where the coke deposition was 7.5% in the spent catalyst. The mole of carbon in each species was found based on its mass fraction and compositions. The carbon yield can be obtained as follows:

$$\text{Carbon yield (\%)} = \frac{C_p + C_G + C_C}{C_F} \times 100\%, \quad (10)$$

where C_F , C_p , C_G , and C_C are the mole of carbon in the feedstock, product, gas, and coke, respectively. The calculations of C_F , C_p and C_G considered the carbon moles in each component within the feedstock, products and gases, respectively.

The energy yield can be calculated as:

$$\text{Energy yield (\%)} = \frac{E_P + E_G}{E_F + E_H + Q} \times 100\%, \quad (11)$$

where E_F , E_H , E_P , and E_G are the energies of feedstock, hydrogen, product, and gases, respectively; Q is the energy input to the reactor. The energies of feedstock, hydrogen, products and gases were determined in accordance with their mass fraction and heating values. The calculation of E_G considered the heating values of each component in the gaseous product. The energy input to the reactor was estimated as the amount of heat transferred to the reactor with the volume of catalytic bed which raised the reaction temperature from room temperature to the desired temperature. As shown in Table 6, the mass, carbon, and energy yields in one and two-step processes were brought into comparison. The two-step process was calculated based on hydro-processing of the palm oil [59] and hydro-isomerization/cracking of the hydro-processed alkanes [60]. The mass, carbon, and energy yields for one-step process are 24.4%, 8.1%, and 10.9% higher than those for two-step process, respectively. It can be seen that the one-step process produces more desired product than the two-step one. In addition, the higher carbon yield indicates that one-step process performs better with regard to carbon footprint. Moreover, higher energy yield points out that one-step process has less energy loss than the two-step one.

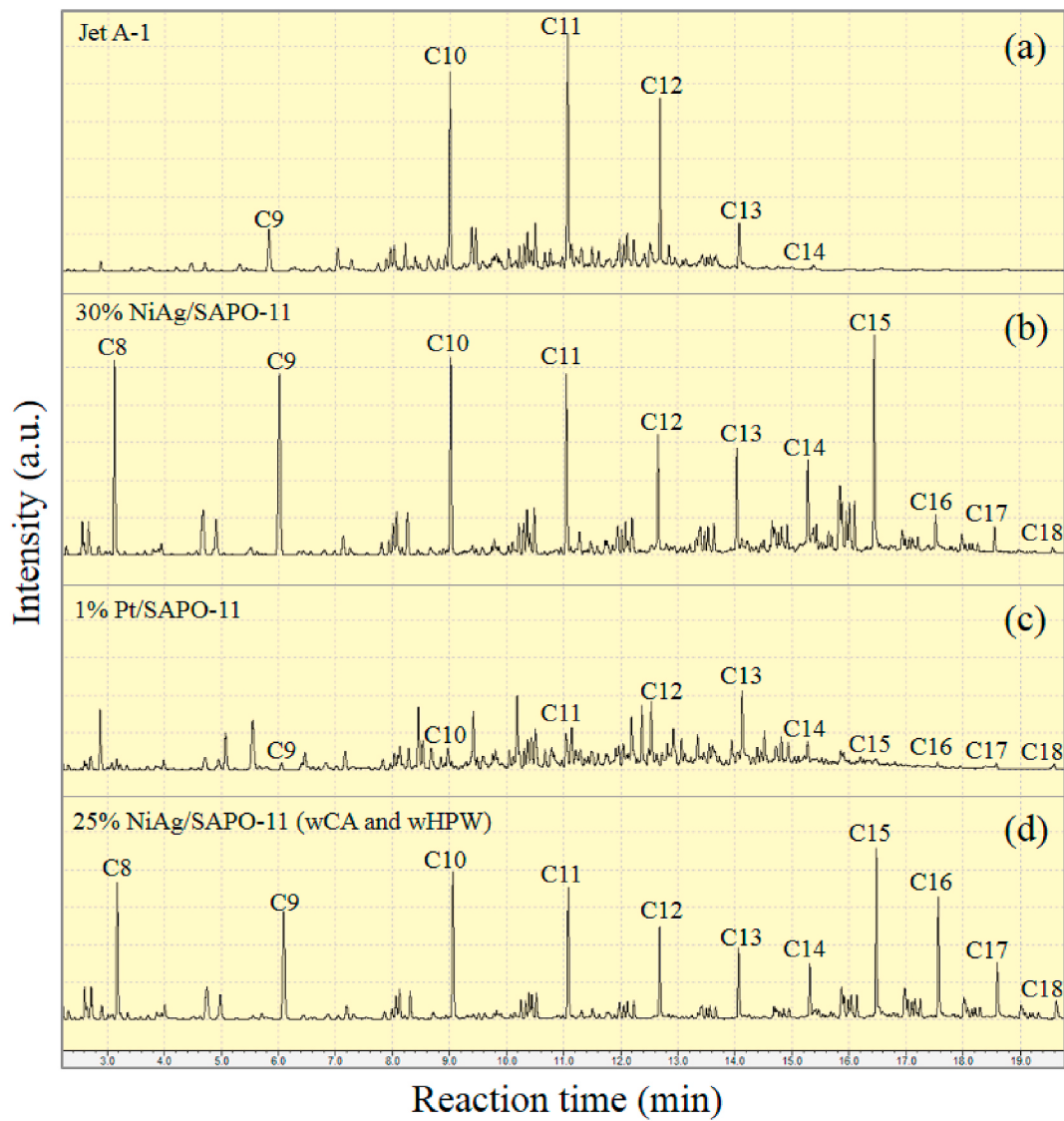


Fig. 15. GC-FID spectra of (a) Jet A-1, (b) HRJ over 30% NiAg/SAPO-11, (c) over 1% Pt/SAPO-11 and (d) over 25% NiAg/SAPO-11 (wCA and wHPW).

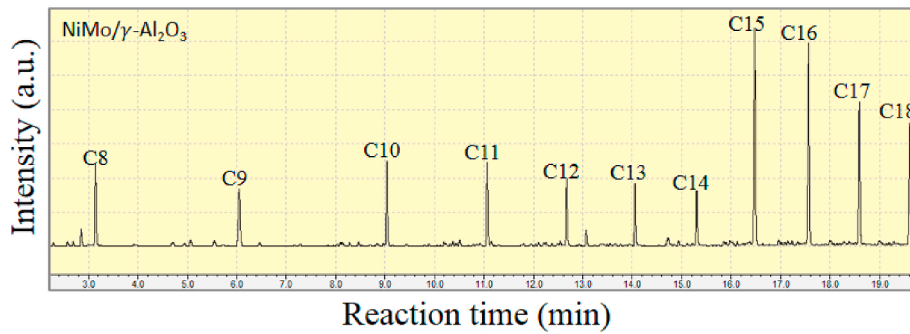


Fig. 16. GC-FID spectrum of hydro-processed alkanes over $\text{NiMo}/\gamma\text{-Al}_2\text{O}_3$.

3.5. Practical implications of this study

This study has presented that the conversion of palm oil into renewable jet fuel through the one-step process has higher mass, carbon and energy yields than the one through the two-step process. In the future work, the one-step HRJ has to be examined through the ASTM D7566 specifications to ensure it meets all the jet fuel requirements. In

addition, the combustion performances such as ignition, flame speed or soot formation for the one-step HRJ could be tested to understand its combustion characteristics. Furthermore, the one-step HRJ should be tested in the real jet engine to see its engine performance and emissions. Moreover, the economics for both one-step and two-step processes could be evaluated and compared for the purpose of process commercialization. The policies regarding the supply and transportation of the palm oil

Table 5
Fuel properties of HRJ-1 and HRJ-2.

Fuel	Property	Yield ^c (%)	
	Aromatics (vol %)	Flash point ^b (°C)	
HRJ-1 ^a	7	58	72
HRJ-2 ^a	9	63	50

^a HRJ-1 and HRJ-2 were fuels produced from the one-step and two-step processes, respectively.

^b Followed ASTM D93 method.

^c The distillation loss was taken into account.

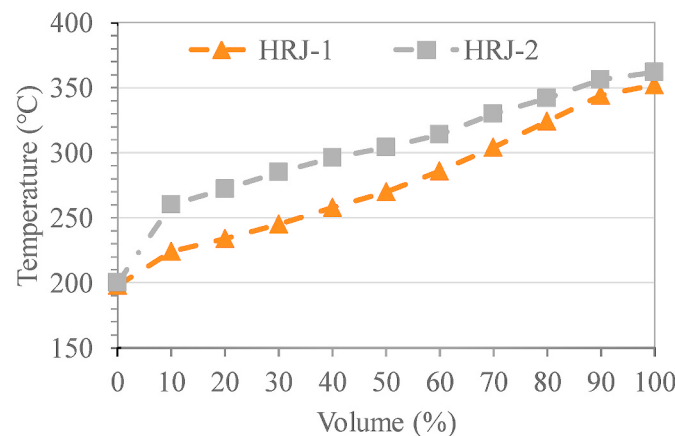


Fig. 17. Distillation curves of HRJ-1 from one-step and HRJ-2 from two-step.

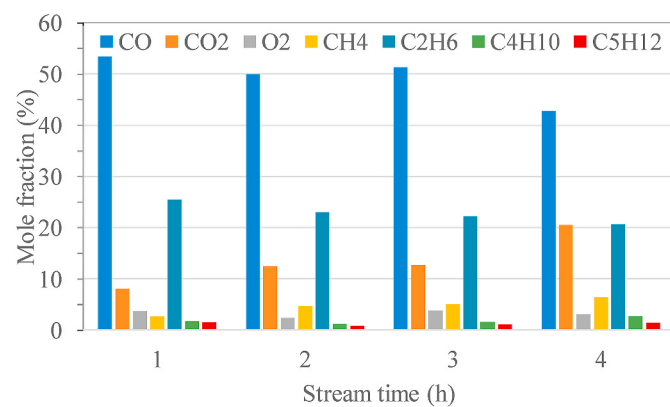


Fig. 18. Gas product distribution of 30% NiAg/SAPO-11 versus stream time. ($T = 400^\circ\text{C}$, $P = 52$ bar, H_2 flow rate = 100 sccm, LHSV = 1 h^{-1}).

Table 6
Mass, carbon, and energy yields.

	Mass yield (%)	Carbon yield (%)	Energy yield (%)
Two-step	58.3	83.9	38.5
One-step	80.0	93.7	48.7

Note: The values in Eqns. (10) and (11) are reported in Table A1 (Supplementary Material).

feedstock should be further implemented in order to support the development of renewable jet fuel. Additionally, the emission factors for aviation using the renewable jet fuels derived by glyceride-based oils have to be established. Therefore, the future work should contain the analyses of energy, economic and environment for this new conversion process.

4. Conclusions

In this study, a Ni-based catalyst was prepared by adding Ag, CA, and HPW as promoters via wetness impregnation. Silver as a strong oxidizer indeed succeeded in removing oxygen from the fatty acids. The XRD, TEM and BET results indicated that smaller Ni particles obtained due to the assistance of CA enlarged the surface area. In the Py-FTIR spectra, the Brønsted and Lewis acid sites were improved with the use of HPW and CA, respectively. The 30% NiAg/SAPO-11 catalyst with good deoxygenation activity, high metal dispersion, and improved isomerization activity showed excellent hydro-conversion performance on the palm oil. High conversion and selectivity of 100% and 84%, respectively, were obtained at the optimal reaction conditions of 400°C , 52 bar, an H_2 flow rate of 100 sccm, and an LHSV of 1 h^{-1} . Also, the content of the iso-alkanes was two times higher than that of the normal alkanes, and 7% aromatics content was obtained. The effect of the iso-alkanes and aromatics content was attributed to the intensity and density of the Brønsted and Lewis acid sites, respectively. The molar ratio of $\text{C}_{15}/\text{C}_{16}$, $\text{C}_{17}/\text{C}_{18}$ and the gas product distribution confirmed that the production of the HRJ mainly depended on decarbonylation and decarboxylation pathways. Based on the distillation curve, the flash point could be determined based on its relationship with the boiling point because the flash point increased with increases in the boiling point. After distillation, the yield of 72% in the one-step process and a flash point of 58°C were obtained. In addition, the mass, carbon and energy yields for the one-step process are higher than the two-step one by 24.4%, 8.1%, and 10.9%, respectively, indicating that the one-step HRJ production process obtains the advantages of production capacity, carbon footprint and energy conversion. This study provides an economic and feasible route to HRJ production from palm oil feedstock in a one-step hydro-conversion process over Ni-based catalysts with high quality and yield.

Credit author statement

Cheng-Han Lin: Conceptualization, Methodology, Validation, Investigation, Writing - original draft, Visualization; Wei-Cheng Wang: Resources, Conceptualization, Methodology, Validation, Investigation, Resources, Data curation, Writing - original draft, Writing - review & editing, Visualization, Supervision, Project administration, Funding acquisition

Declaration of competing interest

The authors declare that they have no known competing financial interests or personal relationships that could have appeared to influence the work reported in this paper.

Acknowledgements

This project was supported by the Ministry of Science and Technology, Taiwan, through grant 108-2221-E-006-220-MY3. The authors are thankful to Prof. Hong-Ping Lin and Mr. Chuan-Lin Zhang for their assistances on catalyst characterizations.

Appendix A. Supplementary data

Supplementary data to this article can be found online at <https://doi.org/10.1016/j.rser.2020.110109>.

References

- [1] Rosillo-Calle F, Teelucksingh S, Thrän D, Seiffert M. The potential role of biofuels in commercial air transport-biojetfuel (No. Task 40: sustainable international bioenergy trade). IEA, Paris 2012.

- [2] 13.04 ExxonMobil. The outlook for energy: a view to 2040. Available, <https://cdn.exxonmobil.com/~media/global/files/outlook-for-energy/2016/2016-outlook-for-energy.pdf>; 2016.
- [3] Van Ruijven B, Van Vuuren DP. Oil and natural gas prices and greenhouse gas emission mitigation. *Energy Pol* 2009;37:4797–808.
- [4] 13.04 IEA. Key World energy statistics 2016. Available, <http://large.stanford.edu/courses/2017/ph241/kwan1/docs/KeyWorld2016.pdf>; 2016.
- [5] 13.04 IATA. Resolution on the implementation of the aviation "CNG2020" strategy. Available, <https://www.iata.org/pressroom/pr/documents/agm69-resolution-cng2020.pdf>; 2010.
- [6] IEA. Technology roadmap biofuels for transport: international energy agency. 13.04. Available, <https://www.fiva.org/wp-content/uploads/Technology-Biofuel-s-for-Transport.pdf>; 2011.
- [7] Kang D, Kim D, Kalaskar V, Violi A, Boehman AL. Experimental characterization of jet fuels under engine relevant conditions – Part 1: effect of chemical composition on autoignition of conventional and alternative jet fuels. *Fuel* 2019;239:1388–404. 2019/03/01.
- [8] Edwards T, Minus D, Harrison W, Corporan E, DeWitt M, Zabarnick S, et al. Fischer-Tropsch jet fuels-characterization for advanced aerospace applications. In: 40th AIAA/ASME/SAE/ASEE joint propulsion conference and exhibit; 2004. p. 3885.
- [9] Shahbandeh M. Palm oil: global production. Stat 2020.
- [10] Zhang C, Hui X, Lin Y, Sung C-J. "Recent development in studies of alternative jet fuel combustion: progress, challenges, and opportunities. *Renew Sustain Energy Rev* 2016;54:120–38. 2016/02/01.
- [11] Dujjanutat P, Kaewkannetra P. "Production of bio-hydrogenated kerosene by catalytic hydrocracking from refined bleached deodorised palm/palm kernel oils. *Renew Energy* 2020;147:464–72. 2020/03/01.
- [12] Li T, Cheng J, Huang R, Yang W, Zhou J, Cen K. "Hydrocracking of palm oil to jet biofuel over different zeolites. *Int J Hydrogen Energy* 2016;41:21883–7. 2016/12/21.
- [13] Krár M, Kovács S, Kalló D, Hancsók J. "Fuel purpose hydrotreating of sunflower oil on CoMo/Al2O3 catalyst. *Bioresour Technol* 2010;101:9287–93.
- [14] Kubíčka D, Kaluža L. Deoxygenation of vegetable oils over sulfided Ni, Mo and NiMo catalysts. *Appl Catal Gen* 2010;372:199–208.
- [15] Senol O, Vilija T-R, Krause A. "Hydrodeoxygenation of methyl esters on sulfidized NiMo/γ-Al2O3 and CoMo/γ-Al2O3 catalysts." *Catalysis Today*, 2005;100:331–5.
- [16] Liu S, Zhu Q, Guan Q, He L, Li W. "Bio-aviation fuel production from hydroprocessing castor oil promoted by the nickel-based bifunctional catalysts. *Bioresour Technol* 2015;183:93–100.
- [17] Coonradt HL, Garwood WE. "Mechanism of hydrocracking. Reactions of paraffins and olefins. *Ind Eng Chem Process Des Dev* 1964;3:38–45.
- [18] Deldari H. "Suitable catalysts for hydroisomerization of long-chain normal paraffins. *Appl Catal Gen* 2005;293:1–10.
- [19] Blasco T, Chica A, Corma A, Murphy W, Agúndez-Rodríguez J, Pérez-Pariente J. Changing the Si distribution in SAPO-11 by synthesis with surfactants improves the hydroisomerization/dewaxing properties. *J Catal* 2006;242:153–61.
- [20] Walendziewski J, Pniak B. "Synthesis, physicochemical properties and hydroisomerization activity of SAPO-11 based catalysts. *Appl Catal Gen* 2003;250: 39–47.
- [21] Shahinuzzaman M, Yaacob Z, Ahmed Y. "Non-sulphide zeolite catalyst for bio-jet-fuel conversion. *Renew Sustain Energy Rev* 2017;77:1375–84.
- [22] Ooi Y-S, Bhatia S. "Aluminum-containing SBA-15 as cracking catalyst for the production of biofuel from waste used palm oil. *Microporous Mesoporous Mater* 2007;102:310–7.
- [23] Twaiq FA, Zabidi NA, Bhatia S. "Catalytic conversion of palm oil to hydrocarbons: performance of various zeolite catalysts. *Ind Eng Chem Res* 1999;38:3230–7.
- [24] Congxin W, Qianhe L, Xuebin L, Lijun Y, Chen L, Lei W, et al. "Influence of reaction conditions on one-step hydrotreatment of lipids in the production of iso-alkanes over Pt/SAPO-11. *Chin J Catal* 2013;34:1128–38.
- [25] Lutz W, Kurzhals R, Sauerbeck S, Toufar H, Buhl J-C, Gesing T, et al. "Hydrothermal stability of zeolite SAPO-11. *Microporous Mesoporous Mater* 2010; 132:31–6.
- [26] Liu Q, Zuo H, Zhang Q, Wang T, Ma L. "Hydrodeoxygenation of palm oil to hydrocarbon fuels over Ni/SAPO-11 catalysts. *Chin J Catal* 2014;35:748–56.
- [27] A. C. D. o. P. Products and Lubricants. Standard specification for aviation turbine fuel containing synthesized hydrocarbons: ASTM international. 2014.
- [28] Bester N, Yates A. Assessment of the operational performance of fischer-tropsch synthetic-paraffinic kerosene in a T63 gas turbine compared to conventional Jet A-1 fuel. In: ASME turbo expo 2009: power for land, sea, and air; 2009. p. 1063–77.
- [29] Rabaev M, Landau MV, Vidruk-Nehemya R, Koukoulev V, Zarchin R, Herskowitz M. "Conversion of vegetable oils on Pt/Al2O3/SAPO-11 to diesel and jet fuels containing aromatics. *Fuel* 2015;161:287–94.
- [30] Corporan E, Edwards T, Shafer L, DeWitt MJ, Klingshirn C, Zabarnick S, et al. "Chemical, thermal stability, seal swell, and emissions studies of alternative jet fuels. *Energy Fuels* 2011;25:955–66.
- [31] Duong LH, Rekswardojo IK, Soerawidjaja TH, Pham DN, Fujita O. "The sooting tendency of aviation biofuels and jet range paraffins: effects of adding aromatics, carbon chain length of normal paraffins, and fraction of branched paraffins. *Combust Sci Technol* 2018;190:1710–21.
- [32] Mukherjee I, Sovacool BK. "Palm oil-based biofuels and sustainability in southeast Asia: a review of Indonesia, Malaysia, and Thailand. *Renew Sustain Energy Rev* 2014;37:1–12. 2014/09/01.
- [33] Zheng S, Kates M, Dubé M, McLean D. "Acid-catalyzed production of biodiesel from waste frying oil. *Biomass Bioenergy* 2006;30:267–72.
- [34] Mancini A, Imperlini E, Nigro E, Montagnese C, Daniele A, Orrù S, et al. "Biological and nutritional properties of palm oil and palmitic acid: effects on health. *Molecules* 2015;20:17339–61.
- [35] Liu Q, Zuo H, Wang T, Ma L, Zhang Q. "One-step hydrodeoxygenation of palm oil to isomerized hydrocarbon fuels over Ni supported on nano-sized SAPO-11 catalysts. *Appl Catal Gen* 2013;468:68–74.
- [36] Yang L, Xing S, Sun H, Miao C, Li M, Lv P, et al. "Citric-acid-induced mesoporous SAPO-11 loaded with highly dispersed nickel for enhanced hydroisomerization of oleic acid to iso-alkanes. *Fuel Process Technol* 2019;187:52–62.
- [37] Cheng J, Zhang Z, Zhang X, Liu J, Zhou J, Cen K. "Hydrodeoxygenation and hydrocracking of microalgae biodiesel to produce jet biofuel over H3PW12O40-Ni/hierarchical mesoporous zeolite Y catalyst. *Fuel* 2019;245:384–91.
- [38] Fan K, Liu J, Yang X, Rong L. "Hydrocracking of Jatropha oil over Ni-H3PW12O40/nano-hydroxyapatite catalyst. *Int J Hydrogen Energy* 2014;39:3690–7.
- [39] Moon K-S, Dong H, Maric R, Pothukuchi S, Hunt A, Li Y, et al. "Thermal behavior of silver nanoparticles for low-temperature interconnect applications. *J Electron Mater* 2005;34:168–75.
- [40] Saggesse C, Singh AV, Xue X, Chu C, Kholghy MR, Zhang T, et al. "The distillation curve and sooting propensity of a typical jet fuel. *Fuel* 2019;235:350–62.
- [41] Pires AP, Han Y, Kramlich J, Garcia-Perez M. "Chemical composition and fuel properties of alternative jet fuels. *BioResources* 2018;13:2632–57.
- [42] Lee SW, Park SD, Kang S, Bang IC, Kim JH. "Investigation of viscosity and thermal conductivity of SiC nanofluids for heat transfer applications. *Int J Heat Mass Tran* 2011;54:433–8.
- [43] Scaldaferri CA, Pasa VMD. "Hydrogen-free process to convert lipids into bio-jet fuel and green diesel over niobium phosphate catalyst in one-step. *Chem Eng J* 2019; 370:98–109.
- [44] Zhang Q, Long K, Wang J, Zhang T, Song Z, Lin Q. "A novel promoting effect of chelating ligand on the dispersion of Ni species over Ni/SBA-15 catalyst for dry reforming of methane. *Int J Hydrogen Energy* 2017;42:14103–14.
- [45] Li X, Chen Y, Hao Y, Zhang X, Du J, Zhang A. "Optimization of aviation kerosene from one-step hydrotreatment of catalytic Jatropha oil over SDBS-Pt/SAPO-11 by response surface methodology. *Renew Energy* 2019;139:551–9.
- [46] Chen Z, Li X, Xu Y, Dong Y, Lai W, Fang W, et al. "Fabrication of nano-sized SAPO-11 crystals with enhanced dehydration of methanol to dimethyl ether. *Catal Commun* 2018;103:1–4.
- [47] Sahoo SK, Ray SS, Singh I. "Structural characterization of coke on spent hydroprocessing catalysts used for processing of vacuum gas oils. *Appl Catal Gen* 2004;278:83–91.
- [48] Huang X, Wang L, Kong L, Li Q. "Improvement of catalytic properties of SAPO-11 molecular sieves synthesized in H2O-CTAB-butanol system. *Appl Catal Gen* 2003; 253:461–7.
- [49] Pu X, Liu N-w, Shi L. Acid properties and catalysis of USY zeolite with different extra-framework aluminum concentration. *Microporous Mesoporous Mater* 2015; 201:17–23.
- [50] Hengsawad T, Srimingkwanchai C, Butnark S, Resasco DE, Jongpatiwut S. "Effect of metal–acid balance on hydroprocessed renewable jet fuel synthesis from hydrocracking and hydroisomerization of biohydrogenated diesel over Pt-supported catalysts. *Ind Eng Chem Res* 2018;57:1429–40.
- [51] Song X, Zhang D. Bimetallic Ag–Ni/C particles as cathode catalyst in AFCs (alkaline fuel cells). *Energy* 2014;70:223–30.
- [52] Dabiri M, Bashiribod S. "Phosphotungstic acid: an efficient, cost-effective and recyclable catalyst for the synthesis of polysubstituted quinolines. *Molecules* 2009; 14:1126–33.
- [53] Xing S, Lv P, Wang J, Fu J, Fan P, Yang L, et al. One-step hydroprocessing of fatty acids into renewable aromatic hydrocarbons over Ni/HZSM-5: insights into the major reaction pathways. *Phys Chem Chem Phys* 2017;19:2961–73.
- [54] Du H, Liu D, Li M, Wu P, Yang Y. Effects of the temperature and initial hydrogen pressure on the isomerization reaction in heavy oil slurry-phase hydrocracking. *Energy Fuels* 2015;29:626–33.
- [55] Chen R-X, Wang W-C. "The production of renewable aviation fuel from waste cooking oil. Part I: bio-alkane conversion through hydro-processing of oil. *Renew Energy* 2019;135:819–35. 2019/05/01.
- [56] Wang C, Tian Z, Wang L, Xu R, Liu Q, Qu W, et al. One-step hydrotreatment of vegetable oil to produce high quality diesel-range alkanes. *ChemSusChem* 2012;5: 1974–83.
- [57] Braun-Unkhoff M, Kathrotia T, Rauch B, Riedel U. About the interaction between composition and performance of alternative jet fuels. *CEAS Aeronaut J* 2016;7: 83–94.
- [58] Vozka P, Šimáček P, Kilaz G. impact of HEFA feedstocks on fuel composition and properties in blends with jet A. *Energy Fuels* 2018;32:11595–606.
- [59] Hsu K-H, Wang W-C, Liu Y-C. Experimental studies and techno-economic analysis of hydro-processed renewable diesel production in Taiwan. *Energy* 2018;164: 99–111. 2018/12/01/.
- [60] Lin C-H, Chen Y-K, Wang W-C. The production of bio-jet fuel from palm oil derived alkanes. *Fuel* 2020;260:116345.